Finite Element Modeling of the Flow of a Rubber Compound Through an Axisymmetric Die Using the CEF Viscoelastic Constitutive Equation

Mir Hamid Reza Ghoreishy, Mojtaba Bagheri-Jaghargh, Ghasem Naderi, Sedigheh Soltani

Iran Polymer and Petrochemical Institute, Tehran 1497713115, Iran

Received 3 August 2011; accepted 12 November 2011
DOI 10.1002/app.36482
Published online 20 February 2012 in Wiley Online Library (wileyonlinelibrary.com).

ABSTRACT: This work is devoted to the simulation of the flow of a high viscosity NR/SBR rubber compound through the die of a single screw extruder with axisymmetric geometry. An in-house developed computer code based on the use of continuous penalty finite element method was employed. Three constitutive equations including two generalized Newtonian models namely; power-law and Carreau and an explicit viscoelastic model named CEF (Criminale-Ericksen-Fillbey) were used to reflect the rheological behavior of the material. Using the parameters of the rheological models determined by a slit die rheometry technique, the flow of the compound was simulated through the die and results were compared with experimentally measured mass flow rates. It is shown that for high viscosity rubber compounds the use of generalized Newtonian models which do not take the normal stress in simple shear flow into consideration gives rise to significant errors in prediction of mass flow rates. On the other hand, comparing the simulations results using the CEF equation with experimental data revealed that this model is the best compromise between generalized Newtonian and full viscoelastic models which need high computational costs and effort.
 J Appl Polym Sci 125: 3648–3657, 2012

Key words: rubber; extrusion; finite element method; viscoelastic; CEF model

INTRODUCTION

Extrusion is one of the major processes of the forming of polymers in which raw materials are plasticated by either a single screw or a twin screw extruder machine and then pressurized and pumped through a die to form into the desired final shape. The quality of the end product is very dependent on polymer melt flow variables such as velocity profile, material orientation, pressure distribution, and temperature field. These parameters are in turn functions of the operating conditions (e.g., screw speed and zone temperatures) and also geometry of the flow domain. Consequently, selecting the proper values for operating conditions and/or optimization of the screw and die geometries will result in the improvement of the product quality, energy saving, and reduction of the manufacturing costs. To achieve these goals, many researchers have tried to develop sophisticated mathematical models to simulate the flow of polymer melts through the screw channel and die using various numerical techniques such as finite volume method (FVM), finite difference method (FDM), and finite element method (FEM). However, among these methods FEM has been extensively used due to its high accuracy and also capability of modeling of intricate geometries. The finite element solutions of the flow equations using the pure viscous rheological models including power-law, Carreau, and the other generalized Newtonian equations have been widely studied. See for example (Ghoreishy et al.[1–3] and Huang et al.[4]). However, the use of complicated constitutive equations, especially viscoelastic models for the flow of rubbery materials in conjunction with finite element method is still a challenging task. For example, Mitsoulis,[5] Marin and Rasmussen,[6] and Ganvier et al.,[7] have taken the advantage of implicit viscoelastic constitutive models. In spite of their high capability in expressing viscoelasticity, the use of implicit models in numerical simulation of the polymer flows is not an easy job. This is because that they add an extra first-order differential equation to the primary set of equations. The solution of first-order differential equations by finite element methods is always associated with the stability and convergence problems. Alternatively, several studies have been carried out using explicit viscoelastic constitutive models. The CEF constitutive equation is one of the very well-known of these series that have been employed by researchers. For example, Ashmore et al.[8] used this model to study coating flows of non-Newtonian fluids. Mitsoulis,[9] took the advantage of this model to simulate the extrudate swell. Norouzi et al.[10] used this equation for the simulation of the

Correspondence to: M. Hamid R. Ghoreishy (M.H.R. Ghoreishy@ippi.ac.ir).

flow in a curved duct with squared cross-section. Bretas et al.[11] in their work applied this constitutive model for the study of the extrusion of different polyethylene blends. In another investigation, Lee et al.[12] used the mentioned constitutive model to study the flow behavior between two concentric rotating spheres. However, based on our literature review no one has used it for the simulation of rubber compounds flow through extruder dies.

In the present study, the flow of a rubber compound through a die of a laboratory extruder with axisymmetric geometry was simulated using an in-house developed computer code based on continuous penalty finite element method under isothermal and steady state conditions. Our preliminary nonisothermal finite element calculations showed that the temperature difference between inlet and outlet of the die is trivial. To prove this we have also experimentally measured the temperature rise along the extruder die. The temperature of the rubber compound at the entry region was recorded using a thermocouple inserted just at the entrance region. The output temperature was also measured by the use of a manual laser type thermometer. It was found that the temperature rise is between 1 and 2°C which justified the assumption of the isothermal condition for the flow under study. Three different constitutive models, namely, two completely viscous (power-law and Carreau) and an explicit viscoelastic equation (CEF) were considered. The results of the simulations were analyzed and compared with the experimental data to check the accuracy of each constitutive model in predicting the process variables.

In the following sections, we first describe the mathematical model and then introduce the three constitutive models used to complete the flow equations. The finite element formulations associated with this problem in conjunction with the developed algorithm for the computer code is briefly described in the next section. The results of the computer simulation for the flow of a rubber compound using the mentioned models through the die of the single screw extruder are presented in the subsequent section. These results are compared with measured output mass flow rates. It is shown that the use of the CEF viscoelastic equation not only gives rise to more accurate results than those obtained by the simple generalized Newtonian models but also complicated algorithms and high computational costs and effort normally required for full implicit viscoelastic constitutive equations are avoided.

Mathematical model

The governing equations of the steady-state, isothermal, and laminar flow of an incompressible non-Newtonian fluid in a two-dimensional cylindrical coordinate system (r, z) (axisymmetric) in the absence of the body forces are given as follows (Bird et al.[13]):

The continuity equation

$$\frac{1}{r}\frac{\partial}{\partial r}(rv_r) + \frac{\partial v_z}{\partial z} = 0 \tag{1}$$

The momentum equation in r direction

$$\rho\left(v_r\frac{\partial v_r}{\partial r} + v_z\frac{\partial v_r}{\partial z}\right) = -\frac{\partial p}{\partial r} - \left[\frac{1}{r}\frac{\partial}{\partial r}(r\tau_{rr}) + \frac{\partial}{\partial z}\tau_{zr} - \frac{\tau_{\theta\theta}}{r}\right] \tag{2}$$

The momentum equation in z direction

$$\rho\left(v_r\frac{\partial v_z}{\partial r} + v_z\frac{\partial v_z}{\partial z}\right) = -\frac{\partial p}{\partial z} - \left[\frac{1}{r}\frac{\partial}{\partial r}(r\tau_{rz}) + \frac{\partial}{\partial z}\tau_{zz}\right] \tag{3}$$

In these equations, v_r and v_z are components of the velocity vector, p is the pressure, ρ is the material density, τ_{rr}, τ_{rz}, τ_{zz} and $\tau_{\theta\theta}$ are the components of the stress tensor $\underline{\underline{\tau}}$ which are normally expressed based on the selected constitutive equations. In this work three constitutive models were chosen which are as follows:

Power-law and Carreau models

For the well-known power-law and Carreau equations which are categorized as the generalized Newtonian models, the stress tensor is expressed in terms of rate-of-deformation tensor $\underline{\underline{\Delta}}$ as:

$$\underline{\underline{\tau}} = -\eta\underline{\underline{\Delta}} \tag{4}$$

The rate-of-deformation tensor for an axisymmetric system is given as:

$$\underline{\underline{\Delta}} = \begin{bmatrix} \Delta_{rr} & \Delta_{r\theta} & \Delta_{rz} \\ \Delta_{\theta r} & \Delta_{\theta\theta} & \Delta_{\theta z} \\ \Delta_{zr} & \Delta_{z\theta} & \Delta_{zz} \end{bmatrix} = \begin{bmatrix} 2\frac{\partial v_r}{\partial r} & 0 & \frac{\partial v_r}{\partial z} + \frac{\partial v_z}{\partial r} \\ 0 & 2\frac{v_r}{r} & 0 \\ \frac{\partial v_r}{\partial z} + \frac{\partial v_z}{\partial r} & 0 & 2\frac{\partial v_z}{\partial z} \end{bmatrix} \tag{5}$$

In eq. (4), η is the shear dependent viscosity which is defined as (Bird et al.[14]):

Power law model

$$\eta = \eta_0\left(\sqrt{\frac{1}{2}I_2}\right)^{n-1} \tag{6}$$

Carreau model

$$\eta = \eta_0\left[1 + \left(\lambda\sqrt{\frac{1}{2}I_2}\right)^2\right]^{\frac{n-1}{2}} \tag{7}$$

TABLE I
Specifications of the Raw Materials

Material	Grade	Density (g cm^{-3})	Mooney viscosity $ML_{(1+4)}$ (100°C)
Natural rubber (NR)	SMR 20 CV	0.91	65
Styrene butadiene rubber (SBR)	1502	0.93	54

In the above equations, η_0 is the consistency of the fluid, n is the power-law index, λ is the relaxation time, and I_2 is the second invariant of the rate-of-deformation tensor given by:

$$I_2 = \left(2\frac{\partial v_r}{\partial r}\right)^2 + \left(2\frac{\partial v_z}{\partial z}\right)^2 + 2\left(\frac{\partial v_r}{\partial z} + \frac{\partial v_z}{\partial r}\right)^2 + \left(2\frac{v_r}{r}\right)^2 \quad (8)$$

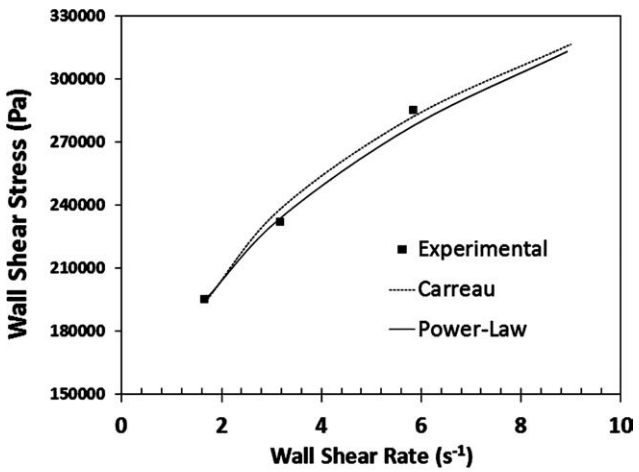

Figure 1 a. Flow curves of the rubber with predicted values by power-law and Carreau models at low shear rates. b. Flow curves of the rubber with predicted values by power-law and Carreau models at high shear rates.

Criminale-Ericksen-Fillbey (CEF) model

The most highlighted weakness of the Generalized Newtonian constitutive models is that they do not take the partly elastic behavior of polymeric materials into account. Conversely, the use of differential or integral viscoelastic equations has intrinsic complications in obtaining stable and accurate results. Therefore, to overcome this problem the elastic behavior of polymer melt was considered using a third constitutive equation which was an explicit viscoelastic model named as CEF model (Bird et al.,[14] Nassehi,[15] Mitsoulis,[16] and Syrjala,[17]) for modeling the flow that do not significantly deviate from viscometric conditions. In this model the stress components are modified to include the influence of the normal stress in non-Newtonian flow behavior (Nassehi,[15]). The components of the stress tensor in this model for an axisymmetric domain are given as (Bird et al.[14]):

$$\tau_{rr} = -2\eta\frac{\delta v_r}{\delta r} - \Psi_2\left(\frac{\delta v_z}{\delta r} + \frac{\delta v_r}{\delta z}\right)^2 \quad (9)$$

$$\tau_{zr} = \tau_{rz} = -\eta\left(\frac{\delta v_z}{\delta r} + \frac{\delta v_r}{\delta z}\right) \quad (10)$$

$$\tau_{\theta\theta} = -2\eta\frac{v_r}{r} \quad (11)$$

$$\tau_{zz} = -2\eta\frac{\delta v_z}{\delta z} - (\Psi_1 + \Psi_2)\left(\frac{\delta v_z}{\delta r} + \frac{\delta v_r}{\delta z}\right)^2 \quad (12)$$

In these equations the partly elastic responses of polymer melt are considered by the first and second normal stress difference coefficients, namely Ψ_1 and Ψ_2. Mitsoulis,[18] proposed that there is very little possibility of secondary flows when there is a main direction for the flow and thus Ψ_2 can be omitted. Consequently, in this work we have neglected the second normal stress coefficient and used the following expression for Ψ_1 suggested by Nassehi[15] given as:

$$\Psi_1 = A\eta^b|\dot{\gamma}_{rz}|^{b-2} \quad (13)$$

where A and b are two material constants which must be determined by an appropriate rheometry technique.

TABLE II
Parameters of the Generalized Newtonian Models (Power-Law and Carreau, SI Unit)

Constitutive model	Low shear rate range			High shear rate range		
	n	η_0	λ	n	η_0	λ
Power-Law	0.28	168,720	–	0.11	236,333	–
Carreau	0.26	242,000	1.6	0.1	81,900	0.3

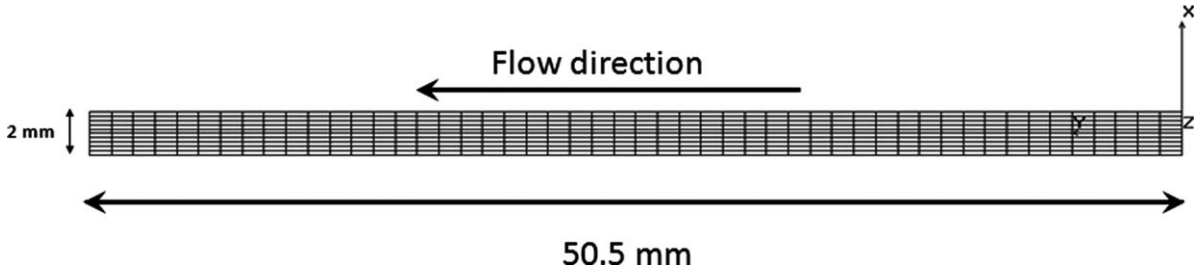

Figure 2 Finite element mesh of the slit die.

Boundary conditions

First type boundary conditions were assumed on both solid walls (no-slip) and symmetry line in which it was supposed there was no cross flow. The mathematical descriptions of these conditions are:

$$\text{On solid walls } v_r = 0, \quad v_z = 0 \tag{14}$$

$$\text{On symmetry line } v_r = 0 \tag{15}$$

Stress free condition (second type boundary condition) was applied on symmetry line of the domain given as follows:

$$\underline{\underline{\tau}}.\underline{n} = 0 \tag{16}$$

where $\underline{n}$ is the unit vector normal to the boundary. Pressure boundary conditions (second type boundary condition) were also imposed at the inlet and outlet of the domain via the finite element working equations described later.

Finite element formulations

The traditional Galerkin finite element method was used to solve the flow equations. The continuous penalty technique was also utilized to handle the incompressibility imposed by the continuity eq. (1). The basic step in the penalty formulation is the elimination of the pressure term in momentum eqs. (2) and (3) using a modified form of the continuity eq. (1) given as:

$$p = -\lambda^* \left[\frac{1}{r} \frac{\partial}{\partial r} (r v_r) + \frac{\partial v_z}{\partial z} \right] \tag{17}$$

where λ^* is the penalty parameter. It can be shown that if we choose λ^* to be a relatively large number, the continuity equation will be satisfied. The value of λ^* is chosen to be a function of viscosity to ensure uniform continuity enforcement in non-Newtonian problems. Therefore it is written as:

$$\lambda^* = \lambda \eta \tag{18}$$

where η is the local viscosity and λ is a very large number. On the basis of our numerical trial and error in this work it is found that a number of 10^{12} gives the most accurate results. Using the Galerkin method, the flow working equations are derived as:

$$\begin{bmatrix} [\mathbf{K}^{11}] & [\mathbf{K}^{12}] \\ [\mathbf{K}^{21}] & [\mathbf{K}^{22}] \end{bmatrix} \begin{Bmatrix} \{\mathbf{v}_r\} \\ \{\mathbf{v}_z\} \end{Bmatrix} = \begin{Bmatrix} \{\mathbf{F}^1\} \\ \{\mathbf{F}^2\} \end{Bmatrix} \tag{19}$$

where $[\mathbf{K}^{11}]$, $[\mathbf{K}^{12}]$, $[\mathbf{K}^{21}]$, and $[\mathbf{K}^{22}]$ are the submatrices of the elemental stiffness matrix; $\{\mathbf{v}_r\}$ and $\{\mathbf{v}_z\}$ are the subvectors of the vector of unknowns and $\{\mathbf{F}^1\}$ and $\{\mathbf{F}^2\}$ are the subvectors of the load vector, respectively. The members of these matrices and vectors are given in the Appendix (Nassehi,[15] and Ghoreishy et al.[1]). Because of the elimination of the pressure from the primary variables, it is calculated by a secondary operation. In this method the pressure of each nodal point was calculated from

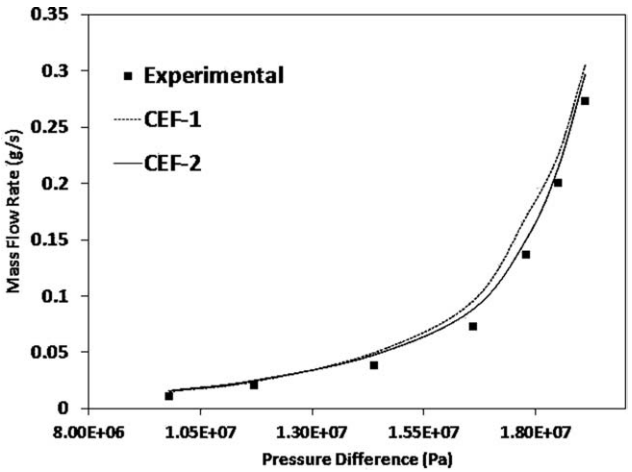

Figure 3 Mass flow rate vs. pressure difference (calculated and experimentally measured) in the slit die used for rheometry.

TABLE III
Parameters of CEF Constitutive Model

Model	Pressure range (Pa)	A (Pa^{1-b} s^{-2})	b
CEF-1	Low ($\leq 1.3 \times 10^7$)	4.5×10^{-7}	2.25
CEF-2	High ($>1.3 \times 10^7$)	3.5×10^{-7}	2.20

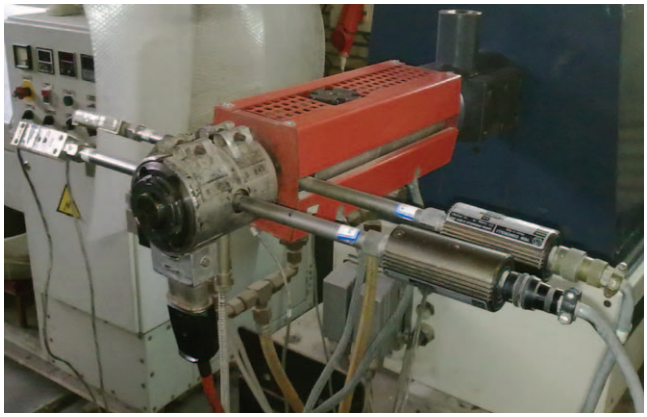

Figure 4 Laboratory extruder used for the extrusion process. [Color figure can be viewed in the online issue, which is available at wileyonlinelibrary.com.]

eq. (A.15), (see Appendix) by averaging the pressure values at four reduced integration points nearest to that node. Having assembled the eq. (19) over a finite element mesh, appropriate boundary conditions are imposed and a set of algebraic equations is obtained. The presence of the convective terms in the momentum as well as the dependency of the local viscosity on the velocity gradients makes this set of equations nonlinear. Consequently, an iterative procedure based on the successive substitution method (Picard's iteration method) (Reddy and Gartling,[19]) has been adopted. The global solution strategy used in this work is based on the method proposed by Sobhani et al.[20]

EXPERIMENTAL

Materials

For the experimental part, a blend of NR and SBR (40/60) was prepared on a Banbury and then a two-roll mill. Table I gives the specifications of the raw materials used in this work. The final compound was rested for 24 h to release elastic memory held in the compound before the rheometry experiments and the extruding operations were carried out.

Rheometry, generalized Newtonian

A slit die rheometry technique was used to study the rheological behavior of the rubber compound. In this technique a low profile with high length slit die was attached to an extruder in conjunction with two pressure transducers installed on the die. Seven screw speeds (1, 2, 4, 8, 16, 24, and 32 RPM) were selected to reproduce the low and high shear rates ranges. The temperature of the rheometry die was also set to 103°C which was the average temperature of the axisymmetric die used for the main extrusion process. The steady state pressure difference and the output mass flow rates associated with each screw speed were measured and recorded. Using the classical flow equations for a slit flow domain,[21] these data were analyzed by the use of a curve-fitting program (Matlab R2007a) and the rheological parameters were determined. Because of the different flow behaviors observed in the rubber compound at low and high shear rates, the curve fitting procedure was carried out for two different shear rate ranges. Figure 1(a,b) illustrate the flow curves of the compound at low and high shear rate regions, respectively, with their corresponding predicted curves by the power-law and Carreau models. The parameters of these models are also listed in Table II.

Rheometry, CEF

Determination of the parameters A and b in the eq. (13) for rubbery materials is not a trivial task. We have used a numerical trial and error approach to find them in which the flow of the rubber through the mentioned slit die was simulated by the use of the finite element method in conjunction with the CEF rheological model in (x,y) coordinate system. Figure 2 shows the finite element mesh used in this calculation. Having used a simple iterative optimization technique, the parameters (A and b) were found so that the error between calculated and experimentally measured output mass flow rates at the each pressure difference became minimum as shown in Figure 3. Similar to generalized Newtonian models, two sets of data were determined at low and high pressure ranges (refer to CEF-1 and CEF-2) which are given in Table III. It follows that the first normal stress coefficient Ψ_1 is also a function of pressure.

Extrusion process

The extrusion process of the rubber compound was carried out using a laboratory single screw extruder. Figure 4 shows the extruder machine with the assembled die and inserted pressure and temperature transducers. The die in this extruder was used to

TABLE IV
Experimental Results of the Rubber Extrusion

Screw speed (RPM)	2	4	6	8	10	12
Entrance pressure (Pa)	5.9×10^6	8.2×10^6	9.2×10^6	10.1×10^6	10.6×10^6	11.0×10^6
Mass flow rate (g s^{-1})	0.051	0.0845	0.121	0.158	0.199	0.245

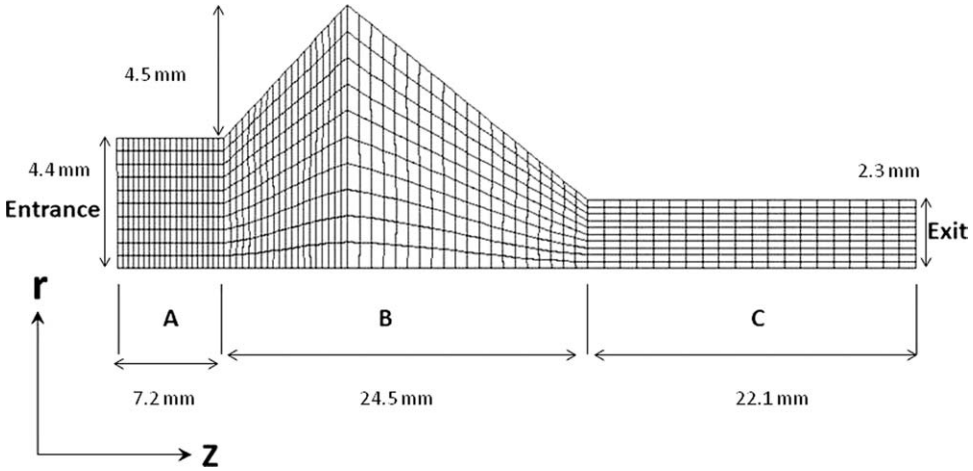

Figure 5 Finite element mesh of the die.

shape the rubber into a rod-type product. Six screw speeds were selected and similar to the rheometry experiment, the entrance pressure and the mass flow rates were measured as recorded in Table IV.

RESULTS AND DISCUSSION

Based on the aforementioned numerical methods an in-house computer code was developed in FORTRAN and used for the simulation of the flow of a rubber compound through the axisymmetric part of the rod die of the extruder shown in Figure 4. The domain of the analysis was discretized into 800 nine-noded quadrilateral elements with 3381 nodes. Figure 5 shows the finite element mesh. Having tried several mesh configurations, the mesh shown in Figure 5 was found to be accurate and convergent.

For each entrance pressure given in Table IV, the simulation was run using both power-law and Carreau constitutive models. The output mass flow rate was calculated from axial component of the velocity vector using the following equation:

$$\dot{M} = 2\pi \int_0^R \rho r v_z dr \tag{20}$$

The comparison between the calculated mass flow rates using eq. (20) and the experimentally measured data in conjunction with the computed errors are illustrated in Figures 6 and 7, respectively. The details of the results obtained by the use of different finite element meshes corresponding to the screw speed of 8 RPM are also given in Table V which confirms the accuracy of the selected mesh shown in Figure 5. As it can be seen in Figures 6 and 7, Carreau constitutive equation gives more accurate results than the power-law model. This is obviously due to taking the initial Newtonian (constant viscosity) behavior of the compound into consideration. However, the errors are still high which can be attributed to the stretching phenomena in polymer

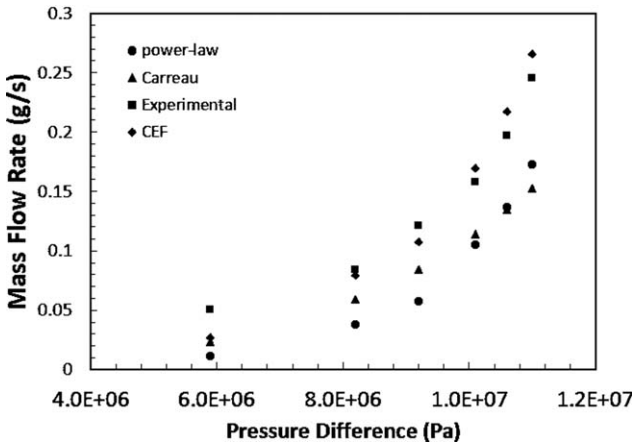

Figure 6 Mass flow rate vs. pressure difference (experimentally measured, predicted by generalized Newtonian models and CEF models) in main extrusion process.

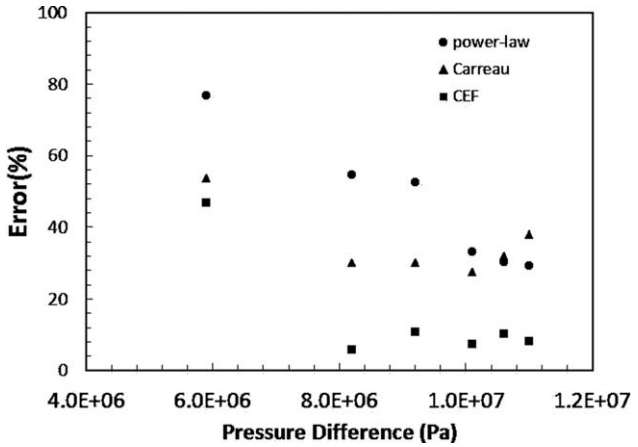

Figure 7 Errors in prediction of the mass flow rates shown in Figure 6.

TABLE V
Computed Mass Flow Rates Using Different Rheological Models with Different Mesh Refinement

			Power-law		Carreau		CEF	
No. of elements	No. of nodes	Flow rate (experimental) (g s^{-1})	Flow rate (g s^{-1})	Error (%)	Flow rate (g s^{-1})	Error (%)	Flow rate (g s^{-1})	Error (%)
32	165	0.158	0.0801	47	0.1115	26	0.180	18
128	585	0.158	0.0931	38	0.1134	25	0.1725	13
512	2193	0.158	0.1071	29	0.1143	24	0.1743	14
800	3381	0.158	0.1054	30	0.1143	24	0.1704	12
1152	4825	0.158	0.1024	32	0.1142	24	0.1716	13

chains during the flow in extruder die especially in rubbery state. This phenomenon generates normal stresses that are not included in the generalized Newtonian models. In other words, pure viscous constitutive models do not completely express all the phenomena happening in the flow of rubber compounds.

To tackle this problem, the simulation of the flow of the rubber compound through the mentioned axisymmetric die was repeated with the CEF constitutive equation. The predicted mass flow rates using the three mentioned models (i.e., power law, Carreau and CEF) in conjunction with experimentally measured data are also shown in Figure 6. Moreover, the errors are compared and illustrated in Figure 7. In addition to the errors of the constitutive equations, they can be attributed to (1) errors associated with the discretization of the equations and (2) the partial slip of the rubber compound on the internal solid wall of the domain which may affect the velocity profile and mass flow rate. It can be seen that the CEF constitutive equation is a more complete rheological model for the flow of the rubber compound so that it can predict the mass flow rate with the calculated errors of even less than 10%. The most logical reason is that CEF equation covers induction of normal stresses in addition to viscous behavior. This can be additionally investigated by the study of the distribution of normal stress in axial direction (τ_{zz}) for a sample screw speed of 8 RPM as shown in Figure 8(a–c). Similar results were obtained for the other screw speeds. While both power-law and Carreau models could predict normal stresses only in the areas where cross section changed (Part B of the die in Fig. 5), the CEF model predicted nonzero normal stress in constant cross section areas which was due to stretching of the macromolecules in those zones. It should be noted that for all rheological models negative values for the τ_{zz} components were obtained at the entrance to the diverging section of the die (Part B). This is because, as rubber molecules enter this section their velocity start decreasing to satisfy the conservation law. Therefore, the molecules with lower velocity push back those with higher values. The

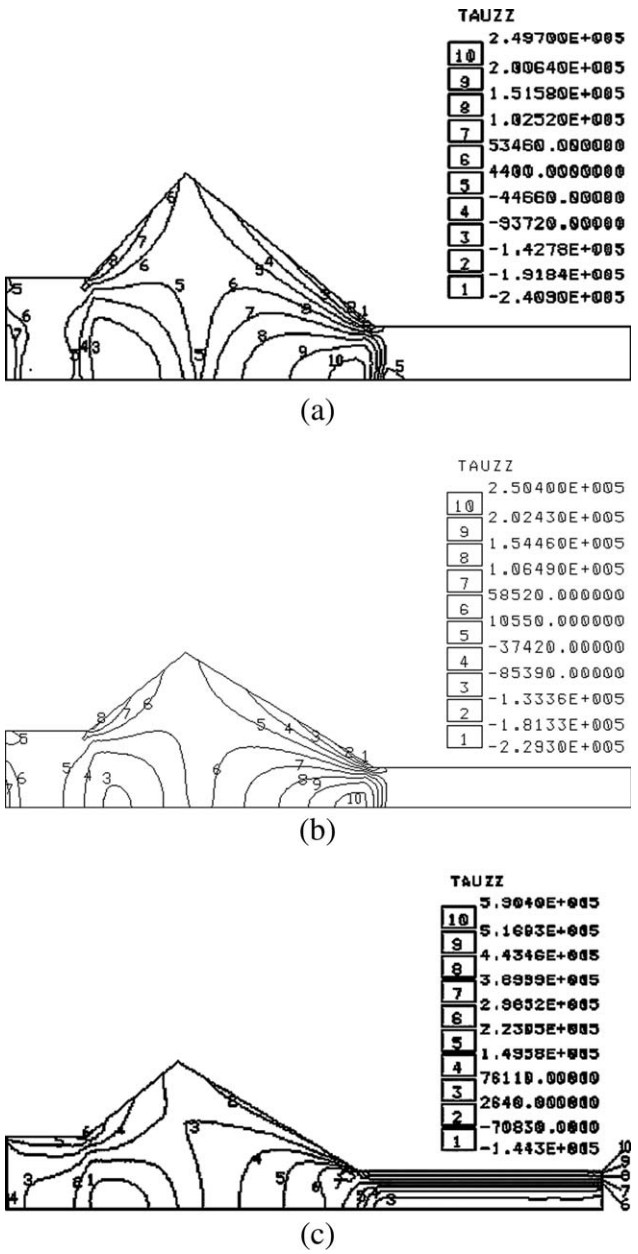

Figure 8 a. Contours of the τ_{zz} predicted by power-law model. b. Contours of the τ_{zz} predicted by Carreau model. c. Contours of the τ_{zz} predicted by CEF model.

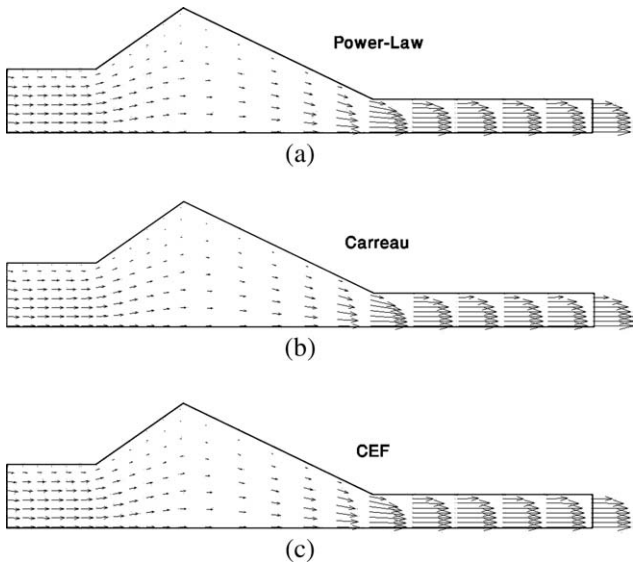

Figure 9 a. Velocity vector in the flow domain predicted by power-law model. b. Velocity vector in the flow domain predicted by Carreau model. c. Velocity vector in the flow domain predicted by CEF model.

consequence is negative values for the τ_{zz} as can be seen in the entrance region of Part B (Fig. 5). In contrast when rubber molecules are leaving this part of the die the normal stress is positive due to the increase in velocity which causes the molecules in higher z implement a positive force on the molecules of lower z. The stress field has also significant impact on the velocity profile. Figure 9(a–c) show the velocity vector field corresponding to screw speed of 8 RPM using the three rheological models, respectively. As it is shown, the overall shapes of the vector fields are similar. However, due to the difference in profile shape and magnitude of stresses (mainly the normal stress), the magnitudes of velocity vectors in each of three areas (A, B, and C shown in Fig. 5) differ for each constitutive model. For this

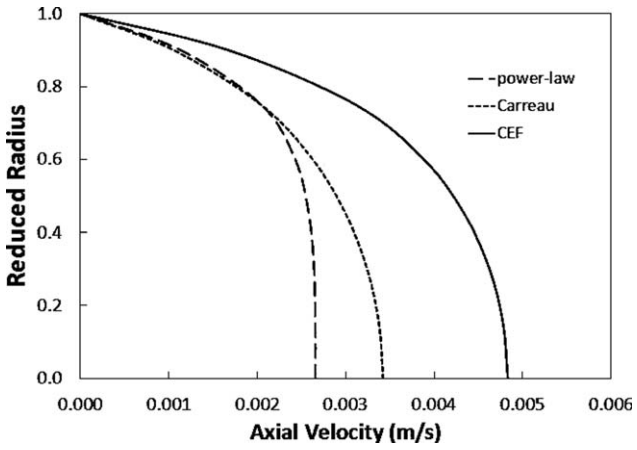

Figure 10 Axial velocity (v_z) profile at zone A (see Fig. 5) of the die.

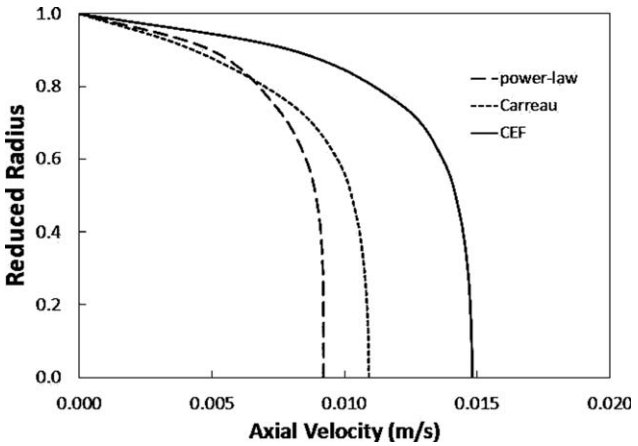

Figure 11 Axial velocity (v_z) profile at zone C (see Fig. 5) of the die.

reason, the integral of the velocity profiles in eq. (19) results in prediction of more accurate of mass flow rates using CEF model. To have a closer look at the effect of the normal stress on the velocity field, the axial velocity profiles in Parts A and C of the die corresponding to screw speed 8 RPM are shown in Figures 10 and 11, respectively. These parts (A and C) have constant cross sections. We can see that due to the existence of the normal stress in CEF model more tension is applied on the flow so that the velocity profile becomes more stretched. In addition, since this tension is parallel to the axial direction it results in larger velocity vectors in that direction. The maximum tension is on the wall which decreases when approaching towards the symmetry line. Therefore, for CEF model the magnitude of axial component of velocity vector near the wall and also its rate of increase is greater than corresponding values predicted by the generalized Newtonian models. This means that the CEF model can predict larger values for the velocity vectors in comparison to power-law and Carreau. This resulted in prediction of larger amounts of mass flow rates which are closer to experimental values.

CONCLUSION

The powerful capabilities of the continuous penalty technique were combined with an explicit viscoelastic constitutive model named CEF equation. A computer program was developed which was used for the simulation of the flow of a high viscosity rubber compound through the die of a single screw extruder with axisymmetric geometry. Two well-known generalized Newtonian models namely: power-law and Carreau equations were also used in the mathematical model. Comparison of the predicted mass flow rates with their associated experimental data revealed that the CEF equation is a very

attractive alternative to both generalized Newtonian and differential and/or integral viscoelastic equations while keeping the computational cost and efforts as low as possible.

APPENDIX

The members of the sub-matrices and sub-vectors in eq. (19) are given as follows:

For generalized Newtonian (power-law and Carreau) models:

$$K_{ij}^{11} = \int_{\Omega_e} \rho\varphi_i\left(\bar{v}_r\frac{\partial\varphi_j}{\partial r}+\bar{v}_z\frac{\partial\varphi_j}{\partial z}\right)d\Omega + \int_{\Omega_e} \eta\left(\frac{2}{r^2}\varphi_i\varphi_j+2\frac{\partial\varphi_i}{\partial r}\frac{\partial\varphi_j}{\partial r}+\frac{\partial\varphi_i}{\partial z}\frac{\partial\varphi_i}{\partial z}\right)d\Omega + \int_{\Omega_e} \lambda\left(\frac{\varphi_i}{r}+\frac{\partial\varphi_i}{\partial r}\right)\left(\frac{\varphi_j}{r}+\frac{\partial\varphi_j}{\partial r}\right)d\Omega \quad (A.1)$$

$$K_{ij}^{12} = \int_{\Omega_e} \eta\frac{\partial\varphi_i}{\partial z}\frac{\partial\varphi_j}{\partial r}d\Omega + \int_{\Omega_e} \lambda\left(\varphi_i\frac{1}{r}\frac{\partial\varphi_j}{\partial z}+\frac{\partial\varphi_i}{\partial r}\frac{\partial\varphi_j}{\partial z}\right)d\Omega \quad (A.2)$$

$$K_{ij}^{21} = \int_{\Omega_e} \eta\frac{\partial\varphi_i}{\partial r}\frac{\partial\varphi_j}{\partial z}d\Omega + \int_{\Omega_e} \lambda\frac{\partial\varphi_i}{\partial z}\left(\frac{\varphi_j}{r}+\frac{\partial\varphi_j}{\partial r}\right)d\Omega \quad (A.3)$$

$$K_{ij}^{22} = \int_{\Omega_e} \rho\varphi_i\left(\bar{v}_r\frac{\partial\varphi_j}{\partial r}+\bar{v}_z\frac{\partial\varphi_j}{\partial z}\right)d\Omega + \int_{\Omega_e} \left(\eta\frac{\partial\varphi_i}{\partial r}\frac{\partial\varphi_j}{\partial r}+2\eta\frac{\partial\varphi_i}{\partial z}\frac{\partial\varphi_j}{\partial z}\right)d\Omega + \int_{\Omega_e} \lambda\frac{\partial\varphi_i}{\partial z}\frac{\partial\varphi_j}{\partial z}d\Omega \quad (A.4)$$

$$F_i^1 = \oint_{\Gamma_e} \varphi_i\left[\left(-p+2\eta\frac{\partial v_r}{\partial r}\right)n_r+\eta\left(\frac{\partial v_z}{\partial r}+\frac{\partial v_r}{\partial z}\right)n_z\right]d\Gamma \quad (A.5)$$

$$F_i^2 = \oint_{\Gamma_e} \varphi_i\left[\eta\left(\frac{\partial v_z}{\partial r}+\frac{\partial v_r}{\partial z}\right)n_r+\left(-p+2\eta\frac{\partial v_z}{\partial z}\right)n_z\right]d\Gamma \quad (A.6)$$

For the CEF:

$$K_{ij}^{11} = \int_{\Omega_e} \rho\varphi_i\left(\bar{v}_r\frac{\partial\varphi_j}{\partial r}+\bar{v}_z\frac{\partial\varphi_j}{\partial z}\right)d\Omega + \int_{\Omega_e} \eta\left(\frac{2}{r^2}\varphi_i\varphi_j+2\frac{\partial\varphi_i}{\partial r}\frac{\partial\varphi_j}{\partial r}+\frac{\partial\varphi_i}{\partial z}\frac{\partial\varphi_j}{\partial z}\right)d\Omega + \int_{\Omega_e} \lambda\left(\frac{\varphi_i}{r}+\frac{\partial\varphi_i}{\partial r}\right)\left(\frac{\varphi_j}{r}+\frac{\partial\varphi_j}{\partial r}\right)d\Omega \quad (A.7)$$

$$K_{ij}^{12} = \int_{\Omega_e} \eta\frac{\partial\varphi_i}{\partial z}\frac{\partial\varphi_j}{\partial r}d\Omega + \int_{\Omega_e} \lambda\left(\varphi_i\frac{1}{r}\frac{\partial\varphi_j}{\partial z}+\frac{\partial\varphi_i}{\partial r}\frac{\partial\varphi_j}{\partial z}\right)d\Omega \quad (A.8)$$

$$K_{ij}^{21} = \int_{\Omega_e} \eta\frac{\partial\varphi_i}{\partial r}\frac{\partial\varphi_j}{\partial z}d\Omega + \int_{\Omega_e} \Psi_1\left(\frac{\partial v_z}{\partial r}+\frac{\partial v_r}{\partial z}\right)\frac{\partial\varphi_i}{\partial z}\frac{\partial\varphi_j}{\partial z}d\Omega + \int_{\Omega_e} \lambda\frac{\partial\varphi_i}{\partial z}\left(\frac{\varphi_j}{r}+\frac{\partial\varphi_j}{\partial r}\right)d\Omega \quad (A.9)$$

$$K_{ij}^{22} = \int_{\Omega_e} \rho\varphi_i\left(\bar{v}_r\frac{\partial\varphi_j}{\partial r}+\bar{v}_z\frac{\partial\varphi_j}{\partial z}\right)d\Omega + \int_{\Omega_e} \left(\eta\frac{\partial\varphi_i}{\partial r}\frac{\partial\varphi_j}{\partial r}+2\eta\frac{\partial\varphi_i}{\partial z}\frac{\partial\varphi_j}{\partial z} + \Psi_1\left(\frac{\partial v_z}{\partial r}+\frac{\partial v_r}{\partial z}\right)\frac{\partial\varphi_i}{\partial z}\frac{\partial\varphi_j}{\partial r}\right)d\Omega + \int_{\Omega_e} \lambda\frac{\partial\varphi_i}{\partial z}\frac{\partial\varphi_j}{\partial z}d\Omega \quad (A.10)$$

$$F_i^1 = \oint_{\Gamma_e} \varphi_i\left[\left(-p+2\eta\frac{\partial v_r}{\partial r}\right)n_r+\eta\left(\frac{\partial v_z}{\partial r}+\frac{\partial v_r}{\partial z}\right)n_z\right]d\Gamma \quad (A.11)$$

$$F_i^2 = \oint_{\Gamma_e} \varphi_i\left[\eta\left(\frac{\partial v_z}{\partial r}+\frac{\partial v_r}{\partial z}\right)n_r + \left(-p+2\eta\frac{\partial v_z}{\partial z}+\Psi_1\left(\frac{\partial v_z}{\partial r}+\frac{\partial v_r}{\partial z}\right)^2\right)n_z\right]d\Gamma \quad (A.12)$$

where φ_i and φ_j are the weight and interpolation functions used to approximate the primary variables over a typical element domain Ω_e by the following expressions:

$$v_r \cong \sum_{j=1}^{N}(v_r)_j\varphi_j \quad (A.13)$$

$$v_z \cong \sum_{j=1}^{N}(v_z)_j\varphi_j \quad (A.14)$$

The pressure at the reduced integration points are also calculated by substituting of the eqs. (A.13) and (A.14) into eq. (17) as:

$$p = -\lambda^*\left(\frac{\bar{v}_r}{r}+\sum_{j=1}^{N}(v_r)_j\frac{\partial\varphi_j}{\partial r}+\sum_{j=1}^{N}(v_z)_j\frac{\partial\varphi_j}{\partial z}\right) \quad (A.15)$$

References

1. Ghoreishy, M. H. R.; Razavi-Nouri, M. J Appl Polym Sci 1999, 74, 676.
2. Ghoreishy, M. H. R.; Razavi-Nouri, M.; Naderi, G. Plast Rubber Compos 2000, 29, 224.
3. Ghoreishy, M. H. R.; Razavi-Nouri, M.; Naderi, G. Comp Mater Sci 2005, 34, 389.
4. Huang, Y.; Gentle, C. R.; Lacey, M.; Prentice, P. Mater Des 2000, 21, 465.
5. Mitsoulis, E. J Non-Newtonian Fluid Mech 2010, 165, 812.
6. Marín, J. M. R.; Rasmussen, H. K. J Non-Newtonian Fluid Mech 2009, 162, 45.
7. Ganvir, V.; Lele, A.; Thaokar, R.; Gautham, B. P. J Non-Newtonian Fluid Mech 2009, 156, 21.
8. Ashmore, J.; Shen, A. Q.; Kavehpour, H. P.; Stone, H. A.; McKinley, G. H. J Eng Math 2008, 60, 17.
9. Mitsoulis, E. Comput Method Appl M 1999, 180, 333.
10. Norouzi, M.; Kayhani, M. H.; Shu, C.; Nobari, M. R. H. J Non-Newtonian Fluid Mech 2010, 165, 323.
11. Bretas, R. E. S.; Granado, C. Eur Polym J 1993, 29, 769.
12. Lee, E.; Lee, Y. H.; Pai, Y. T.; Hsu, J. P. Chem Eng Sci 2002, 57, 507.
13. Bird, R. B.; Stewart, W. E.; Lightfoot, E. N. Transport Phenomena, 2nd ed.; Wiley: New York, 2002.
14. Bird, R. B.; Armstrong, R. C.; Hassager, O. Dynamics of Polymeric Liquids, 2nd ed.; Wiley: New York, 1987.
15. Nassehi, V. Practical Aspects of Finite Element Modeling of Polymer Processing; Wiley: Chichester, 2002.
16. Mitsoulis, E. Polym Eng Sci 1986, 26, 1552.
17. Syrjala, S. Int Commun Heat Mass 1998, 25, 191.
18. Mitsoulis, E. In Encyclopedia of Fluid Mechanics: Polymer Flow Engineering; Cheremisnoff, N. P., Ed.; Gulf Publishing Company: Houston, 1990; Vol. 9, Chapter 21, pp 649–704.
19. Reddy, J. N.; Gartling, D. K. The Finite Element Method in Heat Transfer and Fluid Dynamics, 2nd ed.; CRC Press: New York, 2001.
20. Sobhani, H.; Razavi-Nouri M.; Ghoreishy, M. H. R. J Appl Polym Sci 2011, 120, 1607.
21. Han, C. D. Rheology and Processing of Materials: Polymer Rheology; Oxford University Press: New York, 2007; Vol. 1.